Electronic Supplementary Material (ESI)

for

On-demand, Remote and Lossless Manipulation of Biofluid Droplets

Wei Wang,†[a] Jiefeng Sun,†[b] Sravanthi Vallabhuneni,†[a] Ben Pawlowski,[b] Hamed Vahabi,[b] Kimberly Nellenbach,[cd] Ashley C. Brown,[cd] Frank Scholle,[e] Jianguo Zhao,*[b] Arun K. Kota*[a]

a. *Department of Mechanical and Aerospace Engineering, North Carolina State University, Raleigh, NC 27695, USA. E-mail: akota2@ncsu.edu*

b. *Department of Mechanical Engineering, Colorado State University, Fort Collins, CO 80523, USA. E-mail: jianguo.zhao@colostate.edu*

c. *Joint Department of Biomedical Engineering, North Carolina State University and The University of North Carolina at Chapel Hill, Raleigh, NC 27695, USA.*

d. *Comparative Medicine Institute, North Carolina State University, Raleigh, NC 27695, USA.*

e. *Department of Biological Sciences, North Carolina State University, Raleigh, NC 27695, USA.*

† These authors contributed equally to this work.

*Corresponding authors: *jianguo.zhao@colostate.edu* and *akota2@ncsu.edu*.

This PDF file includes:

Sections S1 to S3

Figures S1 to S3

Movies S1 to S13

Supplementary Text

Section S1. Estimation of the blocking force F_b

To estimate the blocking force F_b, we model the soft manipulator as a planar elastica.[24] This model assumes that the manipulator body undergoes pure bending in a plane and the blocking force is perpendicular to the manipulator tip. We define a centerline curve $s \in [0, L]$, which passes through the centroid of all the cross sections of the manipulator body with an initial length L. Every point along this curve has a position $p \in R^2$ and a rotation $R \in R^{2\times 2}$, relative to a fixed frame at the base of the manipulator. Assuming the elastica is inextensible, the kinematics are given as (Fig. S1a):

$$R(s) = \begin{bmatrix} \cos(\theta) & -\sin(\theta) \\ \sin(\theta) & \cos(\theta) \end{bmatrix} \tag{S1}$$

$$\frac{dR}{ds} = R \begin{bmatrix} 0 & -\frac{d\theta}{ds} \\ \frac{d\theta}{ds} & 0 \end{bmatrix} \tag{S2}$$

$$\frac{d\boldsymbol{p}}{ds} = \begin{bmatrix} -\sin\theta(s) \\ \cos\theta(s) \end{bmatrix} \tag{S3}$$

Here, θ is the angle relative to the vertical axis at a given point s and $\frac{d\theta}{ds}$ is the angular strain of the manipulator body. Considering the statics of the manipulator, based on the moment balance at every point along the manipulator body, we have

$$EI\frac{d\theta}{ds} = M_{block}(s) + M_{act}(s) \tag{S4}$$

Here, E is the Young's modulus of the manipulator, I is the second moment of area for the manipulator cross section, M_{block} is the moment due to the blocking force, and M_{act} is the moment due to the TCA. The moment due to the blocking force M_{block}, which is due to an applied load F_b perpendicular to the tip of the manipulator, can be obtained by multiplying F_b with the distance along the manipulator body from the tip to the point at s,

$$M_{block} = F_b\left[\left(p_x(L) - p_x(s)\right)\sin(\alpha) + \left(p_y(L) - p_y(s)\right)\cos(\alpha)\right] \tag{S5}$$

Here, α is the bending angle at the tip of the manipulator (i.e., $\theta(L) = \alpha$, $p_x(s)$ and $p_y(s)$ are the two components of the position $\boldsymbol{p}(s)$, i.e., $\boldsymbol{p}(s) = \begin{bmatrix} p_x(s) \\ p_y(s) \end{bmatrix}$. Since the moments are not a function of θ, we can take the derivative of Equation S4 to get the moment balance to be dependent only on θ.

$$EI\frac{d^2\theta}{ds^2} = -F_b\cos(\theta - \alpha) + \frac{dM_{act}}{ds} \tag{S6}$$

The distributed moment due to the TCA is a subtle point, which is due to the change in the orientation of the TCA and is given as,

$$\frac{dM_{act}}{ds} = -F_{act}r\frac{d\theta}{ds} \tag{S7}$$

Here, r is the distance from the centerline to the manipulator. Therefore, Equation S6 can be re-written as,

$$EI\frac{d^2\theta}{ds^2} = -F_b\cos(\theta - \alpha) - F_{act}r\frac{d\theta}{ds} \tag{S8}$$

The boundary conditions include the fixed end at the manipulator base and the free end at the manipulator tip. At the fixed end of the manipulator, $\theta(0) = 0$, $p(0) = \begin{bmatrix} 0 & 0 \end{bmatrix}^T$, and $R(0) = \mathrm{diag}([1,1])$. At the free end of the manipulator, $\theta(L) = \alpha$ and $\frac{d\theta}{ds}(L) = 0$. The stiffness EI can be determined using the parallel axis theorem on both of the materials' cross sections (see Fig. S1b),

$$EI = E_1\left(I_{z,1} + A_1 d_1^2\right) + E_2\left(I_{z,2} + A_2 d_2^2\right) \tag{S9}$$

Here, $I_{z,i}$ is the second moment of area of the cross section, E_i is the Young's modulus, A_i is the area of the cross section, and d_i is the distance from the centerline to the center of the cross section for the softer (i = 1) and stiffer (i = 2) layers.

Since the static system of equations is a boundary value problem, we can use a shooting method to solve them numerically by making an initial guess of blocking force F_b and actuation force F_{act} that can be obtained using a physics-based model.[20] The shooting method works by wrapping an initial value problem solver (e.g., a Runge-Kutta integrator) in a root finding method, which solves for the unknown initial conditions (e.g., the blocking force) by repeatedly integrating the ODEs and checking that the boundary conditions are satisfied through the refinement of the guesses. For the statics, we know, $\theta(0)$and $\frac{d\theta}{ds}(L)$ and need to have α to integrate the ODEs. So, we treat $\frac{d\theta}{ds}(0)$ and α as unknown initial conditions. Further, we specify two boundary conditions: the integrated value of $\theta(L)$ must match the guessed α and the calculated $\frac{d\theta}{ds}(0)$ must match the known tip condition, which gives us a fully constrained system. So, given the actuation and blocking forces, we can determine the shape of the manipulator (i.e., solve for $\boldsymbol{p}(s)$) using the shooting method. Subsequently, we approximate the bending curvature κ of the manipulator by taking the computed values of $\boldsymbol{p}$ and fitting a circle passing through three points of the manipulator: the base point $p_1 = \boldsymbol{p}(0)$, the middle point $p_2 = \boldsymbol{p}(L/2)$, and the tip point $p_3 = \boldsymbol{p}(L)$. Using the radius of the fitted circle, we can calculate the curvature as,

$$\kappa = \sqrt{\frac{4x_2^2\left(x_2y_3 - x_3y_3\right)^2}{\left(x_2^2 + y_2^2\right)\left(x_2^2y_3 - x_3^2y_2 + y_2^2y_3 - y_2y_3^2\right)^2}} \tag{S10}$$

Here, we have resolved p_2 and p_3 into their x and y components,

$$p_2 = \begin{bmatrix} p_x\left(\frac{L}{2}\right) \\ p_y\left(\frac{L}{2}\right) \end{bmatrix} = \begin{bmatrix} x_2 \\ y_2 \end{bmatrix},\ p_3 = \begin{bmatrix} p_x(L) \\ p_y(L) \end{bmatrix} = \begin{bmatrix} x_3 \\ y_3 \end{bmatrix} \tag{S11}$$

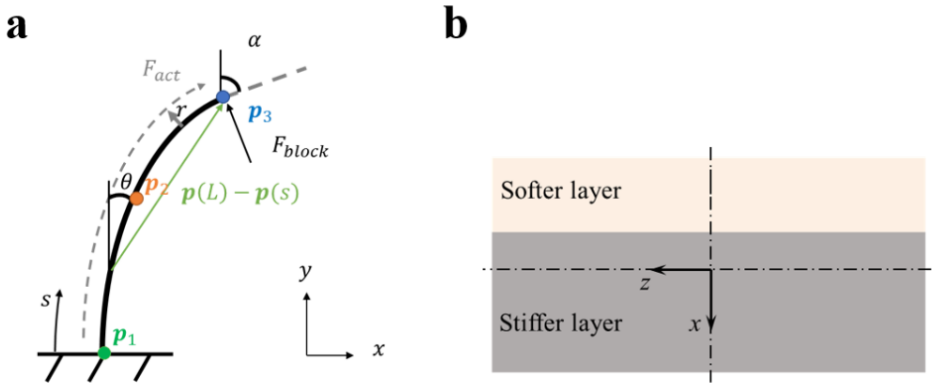

Figure S1. (**a**) Schematic illustrating the elastic model of soft manipulator. (**b**) Schematic illustrating the cross-section of the soft manipulator.

Section S2. Design of the manipulator for simultaneous droplet manipulation

The manipulator for simultaneous droplet manipulation consisted of a single heterochiral TCA in an elliptical shape, with the stiffer elastomer layer facing upward (Fig. S2), so that the two free ends of manipulator can bend upward simultaneously upon actuation.

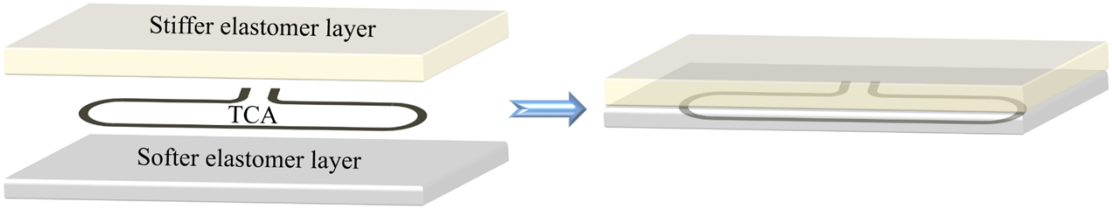

Figure S2. Schematic of the manipulator for simultaneous droplet manipulation.

Section S3. Lossless nature of droplet manipulation and cross-contamination on biofluid manipulators

We evaluated the lossless nature of droplet manipulation and cross-contamination on our biofluid manipulators by measuring the droplet volume, actuator mass and droplet roll off angle as a function of the droplet rastering cycles.

First, we measured the droplet volume and visually inspected the droplets as a function of droplet rastering cycles, sequentially with multiple liquids (hexadecane, water, Bradford reagent, BSA, milk, virus replicon particle laden solution, thrombin, whole blood, fibrinogen and PRP), on a single biofluid manipulator. In each cycle, a 30 μl pendant droplet of the desired liquid was rastered across the surface of the same biofluid manipulator using a linear translation stage. The droplet appearance was inspected, and the droplet image was captured after every 50 cycles and analyzed with ImageJ to determine the droplet volume. Even after 1000 droplet rastering cycles with each liquid, sequentially on the same manipulator, there is neither a significant change in the volume of any droplet (see Figure S3a) nor a discernible change in the appearance of any droplet. These results confirm that there is neither liquid loss nor noticeable cross-contamination associated with our droplet manipulations.

Second, we measured the manipulator mass and visually inspected the manipulator surface as a function of droplet rastering cycles, sequentially with multiple liquids (hexadecane, water, Bradford reagent, BSA, milk, virus replicon particle laden solution, thrombin, whole blood, fibrinogen and PRP), on a single biofluid manipulator. In each cycle, a 30 μl pendant droplet of the desired liquid was rastered across the surface of the same biofluid manipulator using a linear translation stage. The manipulator surface appearance was inspected, and the manipulator mass was measured after every 50 cycles. Even after 1000 droplet rastering cycles with each liquid,

sequentially on the same manipulator, there is neither a significant change in the manipulator mass (see Figure S3b) nor any change in manipulator surface appearance. These results also confirm that there is neither liquid loss nor noticeable cross-contamination associated with our droplet manipulations.

Third, we measured the roll off angles as a function of droplet rastering cycles, sequentially with multiple liquids (hexadecane, water, Bradford reagent, BSA, milk, virus replicon particle laden solution, thrombin, whole blood, fibrinogen and PRP), on a single biofluid manipulator. In each cycle, a 30 µl pendant droplet of the desired liquid was rastered across the surface of the same biofluid manipulator using a linear translation stage. The roll off angle of the liquid (which is very sensitive to surface inhomogeneity) was measured after every 50 cycles. Even after 1000 droplet rastering cycles with each liquid, sequentially on the same manipulator, there is no significant change in the roll off angle of any droplet (see Figure S3c). These results further confirm that there is neither liquid loss nor noticeable cross-contamination associated with our droplet manipulations.

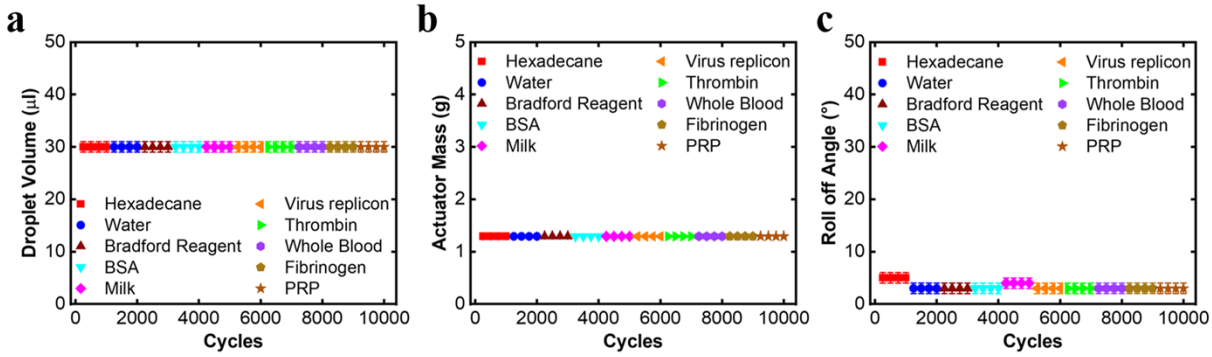

Figure S3. (**a**) Droplet volume as a function of droplet rastering cycles. (**b**) Actuator mass as a function of droplet rastering cycles. (**c**) Droplet roll off angle as a function of droplet rastering cycles.

Movie Legends

Movie S1

Demonstration of large bending angles and quick recovery of soft actuator upon actuation (2X speed).

Movie S2

Bouncing droplets of high and low surface tension liquids (water and hexadecane) on our superomniphobic surfaces (2X speed).

Movie S3

In-plane simultaneous mixing of water droplets (dyed red and blue) using our biofluid manipulator (2X speed).

Movie S4

In-plane simultaneous mixing of n-hexadecane droplets (colorless and dyed red) using our biofluid manipulator (2X speed).

Movie S5

In-plane sequential mixing of water droplets (dyed red, yellow and blue) using our biofluid manipulator.

Movie S6

Out-of-plane manipulation of water droplets (dyed yellow and blue) using our droplet gripper (4X speed).

Movie S7

Out-of-plane manipulation of n-hexadecane droplets (dyed red and colorless) using our droplet gripper (4X speed).

Movie S8

In-plane simultaneous droplet manipulation for protein detection with BSA and Bradford reagent using our biofluid manipulator.

Movie S9

In-plane simultaneous droplet manipulation for protein detection with milk and Bradford reagent using our biofluid manipulator.

Movie S10

In-plane simultaneous droplet manipulation for protein detection with virus-replicon particles and Bradford reagent using our biofluid manipulator.

Movie S11

In-plane simultaneous droplet manipulation for coagulation with whole blood and thrombin using our biofluid manipulator.

Movie S12

In-plane simultaneous droplet manipulation for coagulation with PRP and thrombin using our biofluid manipulator.

Movie S13

In-plane simultaneous droplet manipulation for coagulation with fibrinogen and thrombin using our biofluid manipulator.